

A Novel Photomultiplier Tube Neutron Time-of-Flight Detector

V. Yu. Glebov,¹ C. Stoeckl, C. J. Forrest, J. P. Knauer, O. M. Mannion,
M. H. Romanofsky, T. C. Sangster, and S. P. Regan

Laboratory for Laser Energetics, University of Rochester
250 East River Road, Rochester, NY 14623-1299, USA

ABSTRACT

A traditional neutron time-of-flight (nTOF) detector used in inertial confinement fusion consists of a scintillator coupled with a photomultiplier tube (PMT). The instrument response function (IRF) of such a detector is dominated by the scintillator-light decay. At DT neutron yields larger than 10^{13} a novel detector consisting of a microchannel-plate photomultiplier tube in a housing without a scintillator (PMT nTOF) can be used to measure DT yield, ion temperature, and neutron velocity. Most of the neutron signal in PMT nTOF is produced from neutron interaction with a PMT window. The direct interaction of neutrons with MCP has negligible contribution. The elimination of the scintillator removes the scintillator decay from the instrument response function and makes the IRF of the PMT nTOF faster, which makes the ion temperature and neutron velocity measurements more accurate. Three PMT nTOFs were deployed on the OMEGA Laser System for the first time to diagnose inertial confinement fusion plasma. The design details, characteristics, and calibration results of these detectors in DT implosions on OMEGA are presented. Recommendations on the use of different PMTs for specific applications are provided.

¹ vgle@lle.rochester.edu

I. INTRODUCTION

A traditional neutron time-of-flight (nTOF) detector¹ used in inertial confinement fusion² (ICF) usually consists of a scintillator optically coupled to a photomultiplier tube (PMT). For accurate ion-temperature³ measurements in DT implosions, a scintillator- and PMT-based detector must use a fast scintillator and fast microchannel plate (MCP) PMT. Even with the fastest scintillators, like BC422Q⁴ or EG233Q,⁵ the scintillator light decay significantly contributes to the instrument response function (IRF) of the nTOF detector. The scintillator is necessary for DD and low-DT yield measurements, but the recent DT yield increase on OMEGA and the National Ignition Facility (NIF) stimulated the development of fast, novel detectors without a scintillator such as Cherenkov⁶ and PMT nTOF detectors. A novel PMT nTOF detector developed at Laboratory for Laser Energetics (LLE) has a MCP photomultiplier tube in a housing without a scintillator. This PMT nTOF detector is less sensitive than a traditional nTOF detector with a scintillator and can be used only in high yield, typically larger than 10^{13} DT implosions. Most of the neutron signal in PMT nTOF is produced from neutron interaction with a PMT window. The direct interaction of neutrons with MCP has negligible contribution. Eliminating the scintillator removes the scintillator decay from the IRF and makes the detector faster. The PMT nTOF is the fastest nTOF detector currently in use on OMEGA. The non-scintillator, faster nTOF detectors enable a more-accurate measurement of ion temperature and hot-spot velocity.⁶

The paper is organized as follows: Section II describes several tests studying the origination of the neutron signal in the PMT nTOF and comparing it with the Cherenkov nTOF detector. Section III describes the design and operational performance of nTOF

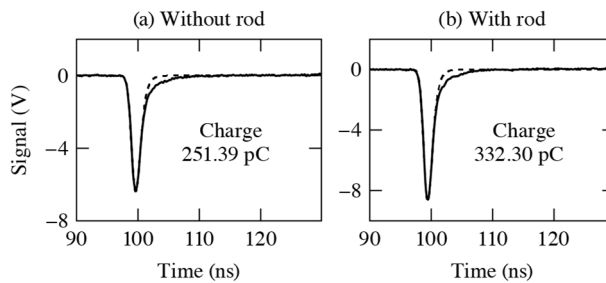
detector based on the Photek⁷ PMT140 photomultiplier. Section IV describes the design and performance of two similar nTOF detectors based on a Hamamatsu⁸ 10-mm MCP PMT. Finally, Section V discusses the recommendations for PMT nTOF applications.

II. PMT nTOF TESTS

The first PMT nTOF tested on OMEGA consists of a Photek⁷ PMT140 photomultiplier housed in thin-wall aluminum housing. The PMT nTOF was tested in the OMEGA Target Bay 5.3 m from the target. Results of these tests were presented⁹ at HTPD 2016 in Madison, WI. At time of the presentation it was initially concluded that the signal in the PMT nTOF detector is produced as a result of direct neutron interaction with the MCP and a new detector was referred to as the MCP nTOF. Later, this detector was moved to 15.9 m from the target and its performance is described in Sec. III.

The second round of the PMT nTOF concept tests was performed on OMEGA during Cherenkov nTOF development on OMEGA. A Cherenkov nTOF detector⁶ (produced by Lawrence Livermore National Laboratory) with a 100-mm-long quartz rod coupled with a Photek⁴ PMT110 gated photomultiplier with a 10-mm-diam photocathode and a single-stage MCP was tested at 5.6 m from the target in the P2 open line of sight (LOS) on OMEGA. The Cherenkov nTOF signal was recorded on a 2.5-GHz, 10-GS/s Keysight DSOS254A oscilloscope. In all scope traces in this paper, the signal amplitude corresponds to the PMT output. The measured neutron temporal trace signal was fit with a convolution of a Gaussian and an exponential decay function, as described in detail in Ref. 10. The fit was performed up to 50% of the falling slope of the signal.

Figure 1 shows a comparison of DT neutron signals recorded by the Cherenkov nTOF detector with and without a 100-mm quartz rod in DT shots with similar yield and ion temperatures. In shot 90972 with a DT yield of 4.17×10^{13} , the Cherenkov detector without a quartz rod recorded a signal with a charge of 251.39 pC. In shot 90976 with a DT yield of 4.30×10^{13} , the Cherenkov detector with a quartz rod recorded a signal with a charge of 332.30 pC. One can calculate from the yields and charges of these two shots that the ratio of without rod to with rod charges equals 0.78. Therefore, in an open, uncollimated LOS where both the quartz rod and PMT are equally exposed to the incident neutrons flux, only about 20% of the signal is produced by quartz rod and about 80% is produced by PMT. The Cherenkov nTOF detector is a truly Cherenkov detector only in a collimated LOS like on the NIF⁶ or at 13 m from target chamber center (TCC) on OMEGA,¹¹ where only the quartz rod is exposed to the incident neutron flux and the PMT is heavily shielded. Since in the open LOS most of the neutron signal is produced by PMT, it is possible to use only the PMT instead of the Cherenkov nTOF detector. Such PMT nTOF detectors are faster than Cherenkov detectors because the timing spread in a quartz rod is eliminated and more sensitive than Cherenkov detectors with a shielded PMT.



E29160J1

FIG. 1. (a) The neutron signal in shot 90972 with a yield of 4.17×10^{13} recorded by a Cherenkov nTOF without a rod. (b) The neutron signal in shot 90976 with a yield of 4.30×10^{13} recorded by a Cherenkov nTOF with a rod.

To determine if the measured neutron signal originates in the window or in the MCP, a comparison test was performed of the PMT nTOF with no gate and with gate (see Fig. 2). The electronic gate energizes the PMT at select times to discriminate unwanted signals. During the shot with the gate, the Photek gate unit produces a 250-V pulse that prevents photoelectrons from the photocathode from reaching the MCP. If a neutron signal is produced by direct interaction of neutrons with the MCP, then the gate will have no effect. However, in shot 91551 with a DT yield of 3.7×10^{13} and no gate pulse in the PMT, the neutron pulse charge was 223.10 pC and in shot 91547 with a DT yield of 4.1×10^{13} and with gate pulse in the PMT, the neutron pulse charge was 5.25 pC. One can calculate from the yields and charges of these two shots that only 2% of the neutron signal is produced by direct interaction with MCP and the remaining 98% of the neutron signal in the PMT nTOF is produced by photoelectrons from the photocathode. The photoelectrons are produced in the PMT fused-silica window in many complex nuclear processes⁶ ranging from (n,γ) interactions and following Compton scattering to “knock-on” O^{16} and Si^{28} ions that produce low-energy electrons in their slowing down.

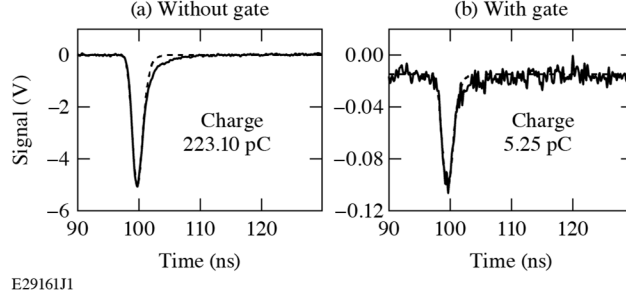


FIG. 2. (a) The neutron signal in shot 91551 with a yield of 3.7×10^{13} recorded by a PMT nTOF with no gate. (b) The neutron signal in shot 91547 with a yield of 4.1×10^{13} recorded by a PMT nTOF with gate.

Every nTOF detector located in an open, uncollimated LOS inside the OMEGA Target Bay records signals from many different radiation sources generated during DT implosion shots. First are hard x rays from laser-plasma interactions; then DT fusion gammas from implosion; then gammas from (n,γ) interactions with diagnostics inside the target chamber; then gammas from (n,γ) interactions with target chamber walls, mirrors support structure, and finally DT fusion neutrons (see scope traces in Fig. 3). The Monte Carlo simulation⁶ shows that fused silica is more sensitive to γ rays than to 14.1-MeV neutrons. If the gain of the PMT is too high, the signals from the gammas may saturate the PMT (deplete the charge) and decrease the DT neutron signal, as is evident by comparing shots 90697 with a DT yield 8.96×10^{13} and shot 90965 with a DT yield of 4.82×10^{13} . The neutron signal amplitude in shot 90697 is ~ 4 V and in shot 90965 the neutron signal amplitude is about 8 V in spite of almost twice the lower yield. This happened because in shot 90697 the PMT was run at much higher gain and gammas

extracted most of the charge from the PMT MCP and it could be recovered before neutrons arrived to PMT. Therefore, for proper operation, the high voltage (HV) on the PMT nTOF should be adjusted in such way that the charge from gamma signals will be about 10% in comparison with the charge from the neutron signal, and the charge from the neutron signal for the maximum desired yield will be less than the saturation level of the PMT.

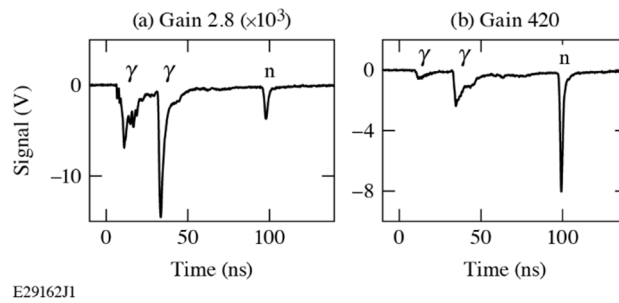


FIG. 3. (a) The neutron signal in shot 90697 with a yield of 8.96×10^{13} recorded by a PMT nTOF with a gain of 2.8×10^3 . (b) The neutron signal in shot 90965 with a yield of 4.82×10^{13} recorded by a PMT nTOF with a gain of 420.

To demonstrate that any PMT can be used as an nTOF detector, a XP2020 dynode PMT without a scintillator was tested in the same LOS as the Cherenkov nTOF and PMT nTOF [see Fig. 4(a)]. The same cables, HV supply, and scope were used in the test. A scope trace from the XP2020 for shot 91970 with a DT yield of 1.51×10^{14} is shown in

Fig. 4(b). The XP2020 was run at a HV of -1.6 kV that is low for this type of PMT. From this scope trace, it is evident that the dynode PMT without a scintillator is sensitive to both gammas and neutrons. But the XP2020 detector is too large, sensitive, slow, and close to the target for 1×10^{14} DT yields on OMEGA. The dynode PMT may be useful to measure DT neutrons in other facilities with lower yields and larger distances from the target.

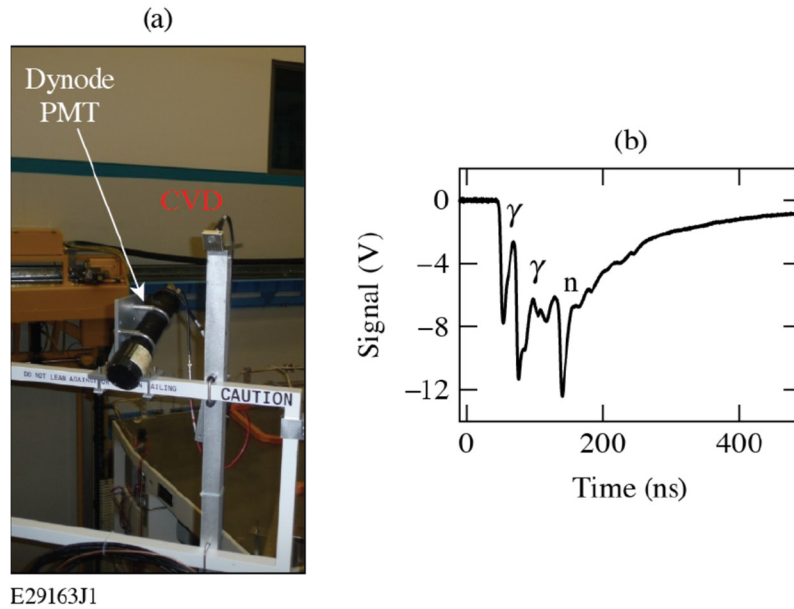


FIG. 4. (a) Photograph of an XP2020 dynode PMT without a scintillator on OMEGA. (b) A scope trace from an XP2020 in shot 91970 with a yield of 1.51×10^{14} .

III. nTOF DETECTOR BASED ON PMT140

After rigorous testing at 5.3 m from the target, the nTOF detector based on Photek⁷ PMT140 was permanently installed on the wall of southeast corner of the OMEGA Target Bay in the P4F line of sight at 15.9 m from the target in order to increase

DT ion temperature accuracy. Figure 5 shows a photo of the installed PMT nTOF detector with the 10-mm-thick lead shielding.



FIG 5. The installed 15.9m PMT nTOF detector with black lead shielding.

The lead shielding and PMT are installed perpendicular to the neutron “beam” from the target. The 15.9m PMT nTOF was tested with and without lead shielding. We are running this detector with lead shielding to suppress gamma signals and increase the dynamic range for neutron signals. A 25-m-long plenum-rated half-inch Heliac cable connects the PMT nTOF detector to a 1-GHz, 10 GS/s Tektronix DPO 7104 oscilloscope. A resistive power divider was used to divide the detector signal among four oscilloscope channels with different sensitivity settings to increase the dynamic range of the recording system.

At 15.9 m the PMT140 is operated at -4.2 kV, corresponding to a PMT gain of 400. The PMT nTOF in this location is capable of measuring DT yields from 1×10^{12} to 3×10^{14} . The neutron signals in shot 85196 with a yield of 9.8×10^{11} and shot 85145 with a yield of 1.5×10^{14} are shown in Fig. 6. The neutron signals from the two shots in Fig. 6 show the minimum and “typical” yields for this detector. The total charge recorded from the PMT140 in shot 85145 is ~ 2 nC that is well below the saturation level¹² of such a PMT. The PMT nTOF at the 15.9-m location was yield-calibrated against the copper

activation diagnostic as shown in Fig. 7(a). The ratio of DT neutron yields measured by the PMT nTOF and the copper activation are shown in Fig. 7(b). The measured neutron yield shot-to-shot precision of the PMT nTOF at the 15.9-m location is better than 1.3%.

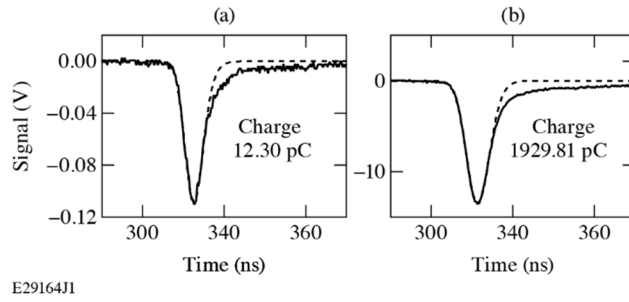


FIG. 6. (a) The neutron signals in shot 85196 with a yield of 9.8×10^{11} recorded by the 15.9mPMT nTOF. (b) The neutron signals in shot 85145 with a yield of 1.5×10^{14} recorded by the 15.9mPMT nTOF.

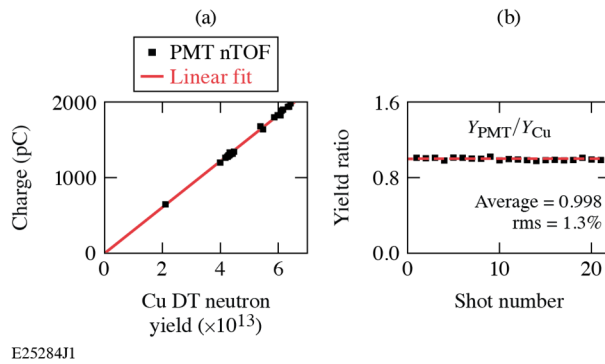


FIG. 7. (a) DT neutron calibration of the 15.9mPMT nTOF against copper activation. (b) The ratio of DT yield measured by the 15.9mPMT nTOF and copper activation.

For ion-temperature calibration of the 15.9mPMT nTOF we used a traditional 15.8m nTOF detector with a 40-mm-diam, 20-mm-thick BC422Q scintillator coupled to a PMT140 and located at 15.8 from TCC. Both detectors use the same type of PMT, the same scopes, located at a similar distance from the target, and the same 10-mm lead front shielding. The only difference between the two nTOF detectors is whether or not a scintillator is included. The comparison of neutron signals recorded on shot 85496 by the 15.8m nTOF detector and the 15.9m PMT nTOF detector is shown in Fig. 8. Shot 85496 used an 860- μm outside diameter, 15- μm -thick CH shell filled with 20 atm of equimolar DT fuel. The ion-temperature distribution is assumed to be isotropic for such shots. The FWHM of the neutron signal recorded by the 15.8m nTOF is 4.31 ns, and the FWHM of the neutron signal recorded by the 15.9m PMT nTOF is 4.11 ns. This comparison demonstrated that the PMT nTOF is faster than a conventional detector with a scintillator.

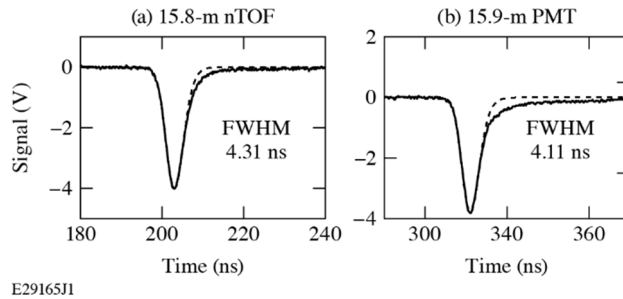


FIG. 8. Neutron signals recorded by the (a) 15.8-m nTOF and (b) 15.9mPMT nTOF on DT shot 85496 with a yield of 3.3×10^{13} and $T_i = 5.1$ keV.

The fitting parameters of the PMT nTOF detector at the 15.9-m location were adjusted to match the ion-temperature measurements of the 15.8m nTOF detector

recorded in room-temperature, thin-shell targets with high-adiabat implosions in which the ion-temperature distribution is considered isotropic. Figure 9(a) shows the ion temperature measured by the PMT nTOF versus the ion temperature measured by the 15.8m nTOF. The ratio of ion temperatures measured by these two similar independent detectors is shown in Fig. 9(b). The standard deviation for the ion temperature ratio is 2.2%, which corresponds to the standard deviation for a single detector of 1.56%. Therefore the ion temperature measurement precision of the 15.9m PMT nTOF is 1.6%.

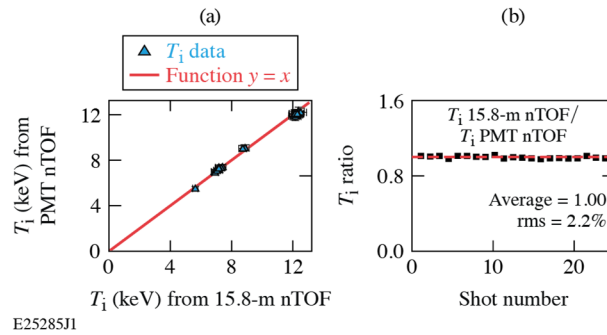


FIG. 9. (a) Ion temperature from the 15.9-m PMT nTOF versus ion temperature from the 15.8-m nTOF. (b) The ratio of ion temperatures from the 15.8-m nTOF and 15.9-m PMT nTOF detectors.

IV. nTOF DETECTORS BASED ON A HAMAMATSU MCP PMT

Two additional fast nTOF detectors were constructed along opposing (antipodal) lines of sight to complete a suite of nTOF detectors on OMEGA for hot-spot-flow velocity measurements.¹³ The H4D and H17E lines of sights were selected for nTOF detector deployment. Since hot-spot flow-velocity measurements require¹³ timing

uncertainties <100 ps, the fastest PMT nTOF based on 10-mm-diam MCP PMTs were selected for these antipodal nTOFs. Two 10-mm-diam Hamamatsu MCP PMTs were available at LLE: one ungated R3809U-52 and one normally gated “OFF” R5916U-50. These are two-stage MCP with gain up to 10^6 . Such high gain is not necessary for a high DT yield on OMEGA, but Hamamatsu produces only two-stage MCP PMTs. A typical PMT nTOF does not require a gate for normal operation. Therefore, the Hamamatsu R5916U-50 PMT has additional complications in comparison with the Hamamatsu R3809U-52. To see any signal from the R5916U-50 PMT one needs a gate pulse with an amplitude of 10 V to 20 V produced by special version of Stanford Research System¹⁴ DG535 delay generator with rear panel output triggered at the exact time. Fortunately, all required hardware was available at LLE and the 500-ns gate pulse was generated, properly timed out, and successfully operated since installation.

To record x-ray IRF from the Hamamatsu PMT during OMEGA timing-calibration shots, each detector has a 1-mm-thick aluminum front PMT housing and each OMEGA sub-port has a 5-mm aluminum window. The ungated R3809U-52 PMT was installed in H4D LOS at 10.4 m from TCC and the gated R5916U-50 PMT was installed at the H17E 4.9 m location. Both detectors were installed with their faces perpendicular to the LOS of the TCC. Photos of two installed PMT nTOF detectors are shown in Fig. 10. Even before installation, it was understood that the H4D 10.4 m location was not the perfect place for the PMT nTOF because it is located too close (~ 10 cm) to the Target Bay wall that produced additional background from (n,γ) interactions. Unfortunately, there were no other options because larger distances from the wall interfered with Target Bay crane operation. To minimize gamma background from (n,γ) interactions with the

Target Bay floor in H17E LOS, we requested a 1-m distance from the floor that led to a 4.9-m distance from TCC. The exact distance of the nTOF detector from TCC is necessary for hot-spot flow-velocity measurements. Therefore, a precision laser-tracking position measurement was performed for each detector to achieve detector LOS distance measurements with uncertainties of ~ 1 mm.

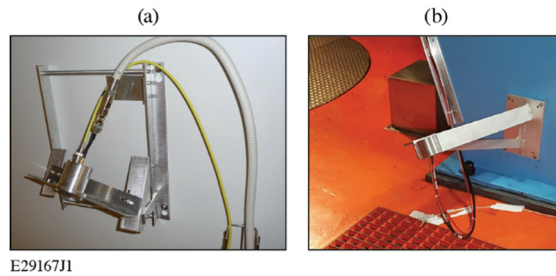


FIG. 10. (a) The H4D PMT nTOF detector at 10.4 m from TCC. (b) The H17E PMT nTOF detector at 4.9 m from TCC.

The H4D detector uses an 18-m-long plenum-rated half-inch Heliac signal cable and the H17E detector uses 15-m LMR-400 signal cables. Each detector uses a Keysight DSOS254A 2.5-GHz, 20-Gs/s scope for signal recording. A resistive power divider was used to divide the detector signal among three oscilloscope channels with different sensitivity settings to increase the dynamic range of the recording system. The absolute timing of the neutron signal is accomplished by recording the OMEGA optical fiducial pulse train¹⁵ in the fourth scope channel in each scope.

The HV setting (PMT gain) for the H4D and the H17E PMT nTOF detectors were selected during high-DT yield shots on OMEGA. The HV setting for each detector was

gradually decreased from shot to shot until signals from (n,γ) interactions were sufficiently small compared to the DT fusion neutron signal. The second requirement in HV setting is that the total charge from all sources at maximum desired yield should be less than the PMT saturation limit. For a 10-mm MCP PMT this limit is about 1 nC. After such adjustment process, the HV setting for both detectors was -2.0 kV with a very low PMT gain of about 100. Examples of the scope trace from the H4D and H17E PMT nTOF detectors for shot 93868 with a yield of 1.4×10^{14} are shown in Fig. 11. The total charge for the H4D detector is 292.98 pC and for the H17E detector is 396.20 pC. Both detectors are well below the charge saturation limit and should measure 2×10^{14} DT yields without saturation.

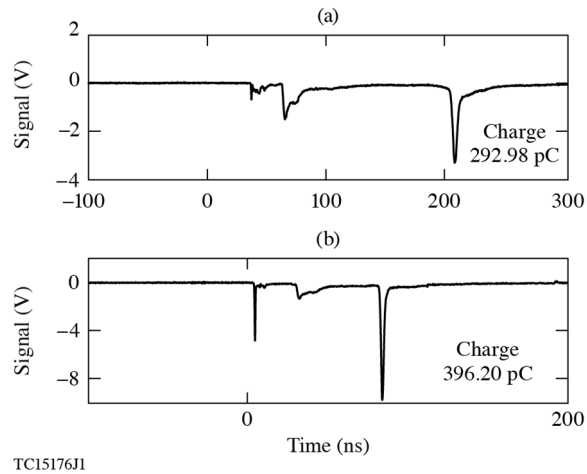


FIG. 11. The scope traces from (a) H4D and (b) H17D PMT nTOF detectors for shot 93868 with a yield of 1.4×10^{14} .

The neutron instrument response function (IRF) is very important for accurate measurement of the neutron energy and hot-spot flow-velocity¹³ in DT implosions. Since in the absence of short impulse of 14 MeV neutrons it is impossible to measure neutron IRF directly, a two-step process described in details in Ref. 16 was used. On the first step, an x-ray IRF was experimentally measured and on the second step the neutron IRF was constructed by correcting x-ray IRF for the DT neutron propagation time modeled in MCNP (Monte Carlo N-Particle code).

The x-ray IRF for the H4D and the H17E PMT nTOF detectors were measured with a 100-ps laser pulse on a gold target. The measured x-ray signals are aligned in time and are averaged to generate the detector IRF. Additionally, the x-ray measurements along with accurate laser timing enables these detectors to have total timing uncertainty¹³ of ~ 60 ps. With the 55 laser beams on a gold target, the H17E PMT nTOF at 4.9 m from TCC recorded an 8-V x-ray signal and H4D PMT nTOF at 10.4 m from TCC recorded a 0.8-V x-ray signal. Results of these measurements normalized to 1.0 for each shot are shown in Fig. 12. Both detectors have subnanosecond x-ray IRF: the H4D nTOF has 540 ± 20 ps FWHM and the H17E nTOF has 360 ± 12 ps FWHM. The uncertainty on the IRF FWHM is taken from the standard error of the mean FWHM from the set of IRF measurements. The 14-MeV neutrons propagation time through 3.2-mm thick PMT window is very short (62 ps) and convolution of x-ray with MCNP simulation is practically the same as x-ray IRF. Using the constructed neutron IRF, the hot-spot flow velocity in DT fusion experiments can be determined from the H4D and the H17E PMT nTOF signals using a forward-fitting method.¹⁶ The H4D and H17E forward fit for shot 95201 with a yield of 1.1×10^{14} , and a T_i of 4.3 keV is shown in Fig. 13. The PMT

nTOF detector in the H17E location has a negligible background and a good fit is achieved with only the IRF. The PMT nTOF detector in the H4D location has an additional gamma background from (n,γ) interactions with the Target Bay wall. For proper fitting of a neutron peak, a modified Gaussian background contribution is included in the forward fit and determined on each shot [see Fig 13(a)].

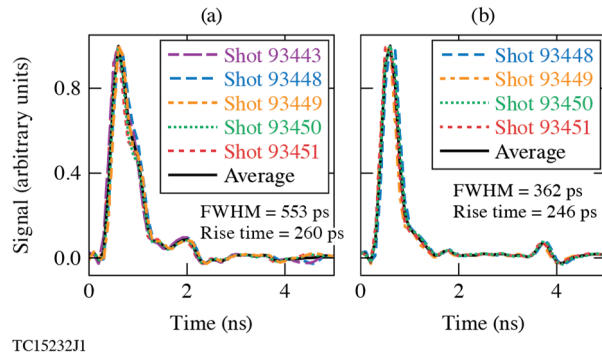


FIG. 12. The x-ray IRF for (a) H4D and (b) H17E nTOF detectors.

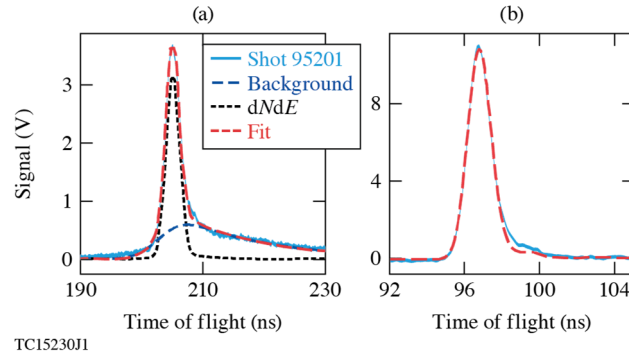


FIG. 13. The forward fit of neutron signals from (a) H4D and (b) H17E nTOF detectors.

The commissioning of the H4D and H17E PMT nTOF detectors completed the suite of nTOF detectors on OMEGA for hot-spot motion measurements.¹³ Now the hot-spot flow velocity is routinely measured for all DT cryogenic and room-temperature target implosions with high-DT yield. Figure 14 shows a Mollweide projection of the OMEGA target chamber coordinate system with the neutron-averaged hot-spot velocity reconstruction for two shot days with exploding-pusher and cryogenic implosions. The size of the stars are proportional to the magnitude of the velocity reconstruction. The OMEGA port locations and stalk positions are shown for reference. The detailed description of the full suite of nTOF detectors used for hot-spot motion measurements, velocity-reconstruction procedure, and data analysis can be found in Ref. 13.

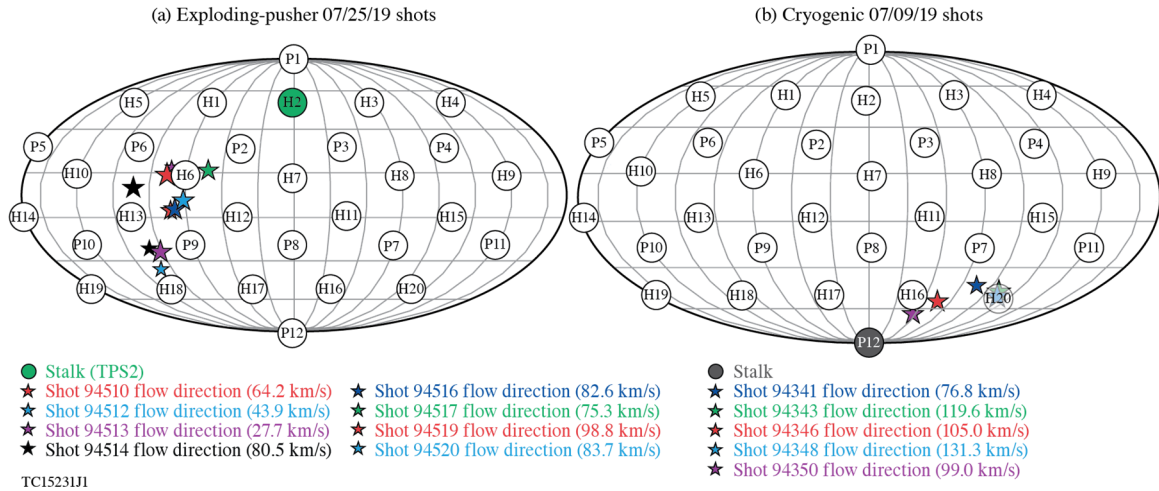


FIG. 14. A Mollweide projection of the OMEGA target chamber coordinate system with the neutron-averaged hot-spot velocity reconstruction. (a) Exploding-pusher 07/25/19 shots. (b) Cryogenic 07/09/19 shots.

In addition to measuring the hot-spot motion, the H4D and H17E PMT nTOF detectors are used to measure yield and ion temperature in DT implosions on OMEGA. Both detectors were calibrated in the room-temperature, thin-shell targets with high-adiabat implosions in which the yield and the ion-temperature distribution is considered isotropic. Figure 15 shows results for DT yield calibration on OMEGA against the Cu activation diagnostic. Figure 16 shows the T_i measured by the H4D and H17E detectors compared with the T_i measured by the Petal nTOF detector.¹⁷ The operational yield range for the H4D and H17E PMT nTOF detectors is from 1×10^{13} to 2×10^{14} .

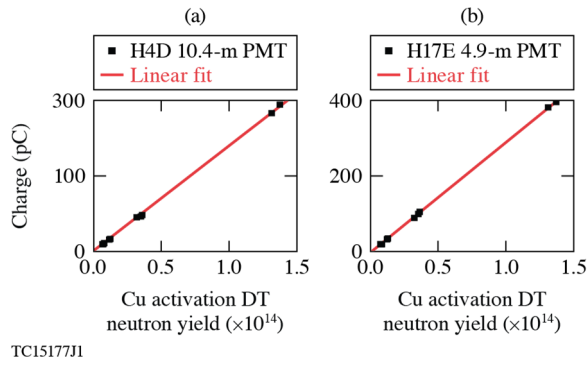


FIG. 15. The (a) H4D and (b) H17E nTOF detectors were calibrated for DT yield against Cu activation.

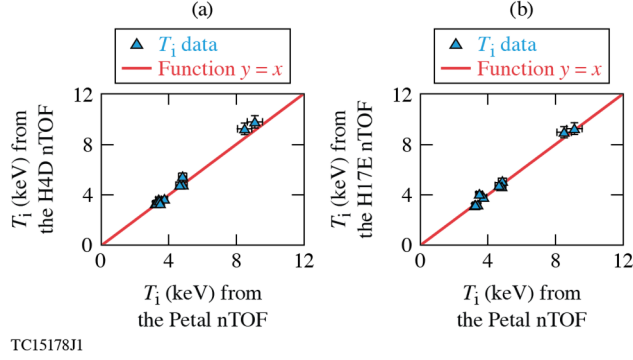


FIG. 16. The T_i measured by the (a) H4D and (b) H17E nTOF detectors were compared with the T_i measured by the Petal nTOF detector.

V. DISCUSSION AND RECOMMENDATION

Any PMT can be used as an nTOF detector in a high-yield DT implosion. But from practical point of view, the most interesting are fast MCP PMT's. Since the PMT nTOF usually operates at very low HV, there is a large reserve in PMT gain and the sensitivity of the PMT nTOF is determined by number of neutron interactions in the PMT window or photocathode diameter. MCP PMTs with a larger photocathode are more sensitive, but slower than a MCP PMT with a smaller photocathode. The commercially available set of MCP PMTs make it possible to design a PMT nTOF for the specific facility distance and yield range. The fastest MCP PMTs are the 10-mm-diam photocathode Hamamatsu⁵ R3809U-52 and Photek⁴ PMT110. Next in line are the Photek PMT125 and PMT140 with 25-mm and 40-mm-diam photocathodes. One of these four types of MCP PMTs can be chosen depending on the particular neutron-yield range and available distance from the target. There is a weak dependence of the number of photoelectrons created by neutrons in the PMT from glass window and photocathode

material and dependence of gain from MCP parameters. But to study all these dependences is economically challenging because MCP PMT is very expensive. And on another hand all such material optimization doesn't make sense because any possible optimization can be much easier achieved by small HV (gain) adjustment. The PMT nTOF can be used both in collimated and uncollimated (open) LOS. In an open LOS, the operational HV or PMT gain should be selected to make the gamma signal contribution from (n,γ) interactions with the target chamber small ($\sim 10\%$) in comparison to the DT neutron signal and not saturate the PMT at the maximum designed yield. To avoid additional background to the neutron signal from (n,γ) interactions, there should be no massive objects in at least 1 m from the PMT. After following these recommendations, the resulting fast PMT nTOF detector will measure DT yield, ion temperature, and, in combination with other nTOF detectors, the hot-spot motion in an ICF implosion.

ACKNOWLEDGMENT

This material is based upon work supported by the Department of Energy National Nuclear Security Administration under Award Number DE-NA0003856, the University of Rochester, and the New York State Energy Research and Development Authority.

This report was prepared as an account of work sponsored by an agency of the U.S. Government. Neither the U.S. Government nor any agency thereof, nor any of their employees, makes any warranty, express or implied, or assumes any legal liability or responsibility for the accuracy, completeness, or usefulness of any information, apparatus, product, or process disclosed, or represents that its use would not infringe

privately owned rights. Reference herein to any specific commercial product, process, or service by trade name, trademark, manufacturer, or otherwise does not necessarily constitute or imply its endorsement, recommendation, or favoring by the U.S. Government or any agency thereof. The views and opinions of authors expressed herein do not necessarily state or reflect those of the U.S. Government or any agency thereof.

DATA AVAILABILITY

The data that support the findings of this study are available within the article.

REFERENCES

1. V. Yu. Glebov, T. C. Sangster, C. Stoeckl, J. P. Knauer, W. Theobald, K. L. Marshall, M. J. Shoup III, T. Buczek, M. Cruz, T. Duffy, M. Romanofsky, M. Fox, A. Pruyne, M. J. Moran, R. A. Lerche, J. McNaney, J. D. Kilkenny, M. J. Eckart, D. Schneider, D. Munro, W. Stoeffl, R. Zacharias, J. J. Haslam, T. Clancy, M. Yeoman, D. Warwas, C. J. Horsfield, J.-L. Bourgade, O. Landoas, L. Disdier, G. A. Chandler, and R. J. Leeper, *Rev. Sci. Instrum.* **81**, 10D325 (2010).
2. J. D. Lindl, *Inertial Confinement Fusion: The Quest for Ignition and Energy Gain Using Indirect Drive* (Springer-Verlag, New York, 1998).
3. V. Yu. Glebov, C. Stoeckl, T. C. Sangster, S. Roberts, G. J. Schmid, R. A. Lerche, and M. J. Moran, *Rev. Sci. Instrum.* **75**, 3559 (2004).
4. Saint-Gobain Crystals, Hiram, OH 44065, Accessed 2 September 2020, <http://www.crystals.saint-gobain.com>
5. Eljen Technology, Sweetwater, TX 79556, Accessed 2 September 2020, www.eljentechnology.com

6. A. S. Moore, D. J. Schlossberg, E. P. Hartouni, D. Sayre, M. J. Eckart, R. Hatarik, F. Barbosa, J. Root, C. Waltz, B. Beeman, M. S. Rubery, and G. P. Grim, *Rev. Sci. Instrum.* **89**, 10I120 (2018).
7. Photek Ltd., St. Leonards on Sea, East Sussex, TN38 9NS, United Kingdom.
8. Hamamatsu Photonics K.K., Hamamatsu City, Shizuoka, Japan 4308587.
9. V. Yu. Glebov, R. Flight, C. J. Forrest, J. P. Knauer, S. P. Regan, M. H. Romanofsky, T. C. Sangster, and C. Stoeckl, presented at the 21st Topical Conference on High-Temperature Plasma Diagnostics 2016, Madison, WI, 5–9 June 2016.
10. T. J. Murphy, R. E. Chrien, and K. A. Klare, *Rev. Sci. Instrum.* **68**, 610 (1997).
11. V. Yu. Glebov, M. J. Eckart, C. J. Forrest, G. P. Grim, E. P. Hartouni, R. Hatarik, J. P. Knauer, A. S. Moore, S. P. Regan, T. C. Sangster, D. J. Schlossberg, and C. Stoeckl, *Rev. Sci. Instrum.* **89**, 10I122 (2018).
12. J. S. Milnes, T. M. Conneely, C. J. Horsfield, and J. Lapington, *Rev. Sci. Instrum.* **89**, 10K104 (2018).
13. O. M. Mannion, J. P. Knauer, V. Yu. Glebov, C. J. Forrest, A. Liu, Z. L. Mohamed, M. H. Romanofsky, T. C. Sangster, C. Stoeckl, and S. P. Regan, *Nucl. Instrum. Methods Phys. Res. A* **964**, 163774 (2020).
14. Standard Research Systems Inc., Sunnyvale, CA, 94809-2279, Accessed 2 September 2020, <https://www.thinksrs.com/>.
15. C. Stoeckl, V. Yu. Glebov, J. D. Zuegel, D. D. Meyerhofer, and R. A. Lerche, *Rev. Sci. Instrum.* **73**, 3796 (2002).

16. R. Hatarik, D. B. Sayre, J. A. Caggiano, T. Phillips, M. J. Eckart, E. J. Bond, C. Cerjan, G. P. Grim, E. P. Hartouni, J. P. Knauer, J. M. Mcnaney, and D. H. Munro, *J. Appl. Phys.* **118**, 184502 (2015).
17. O. M. Mannion, V. Yu. Glebov, C. J. Forrest, J. P. Knauer, V. N. Goncharov, S. P. Regan, T. C. Sangster, C. Stoeckl, and M. Gatu Johnson, *Rev. Sci. Instrum.* **89**, 10I131 (2018).